

Aerodynamic Optimization of the ERICA Tilt-Rotor Intake and Exhaust System

A. Garavello¹, E. Benini², R.Ponza³, A.Scandroglio⁴, A.Saporiti⁵

¹ Research Engineer, University of Padova, HIT09 Srl, garavello.stage@agustawestland.com

² Associate Professor, University of Padova, HIT09 Srl, ernesto.benini@unipd.it

³ Research Engineer, HIT09 Srl, r.ponza@hit09.com

⁴ Aerodynamics Senior Specialist, AgustaWestland, alessandro.scandroglio@agustawestland.com

⁵ Aerodynamics Manager, AgustaWestland, antonio.saporiti@agustawestland.com

Aerodynamic design and optimization of engine installation have recently become of relevant interest for helicopter manufacturers, in particular for heavy helicopters and tilt-rotors. In fact total pressure loss reduction, together with the optimization of the flow pattern at the engine aerodynamic interface plane, increases the global engine efficiency and results in lower fuel consumption. At the same time, a reduction of the engine exhaust back pressure corresponds to an increase of the engine power output that is particularly valuable in hover flight condition. In such context the application of advance optimization algorithms coupled with CFD solvers for the accurate flow solution represents a very powerful tool for parametric design and optimization of engine installation. Because of the above mentioned reasons, the consortium constituted by the University of Padova (UNIPD) and the spin-off company HIT09 developed an automatic optimization loop, based on the home made genetic algorithm GDEA, applicable to engine installation design as well as to general aircraft and rotorcraft components optimization problems. The application of the GDEA-based optimization loop to the ERICA tilt-rotor air intake system is fully described in this paper and the results here presented demonstrate the effectiveness of parametric design and optimization methods in solving engine installation design problems.

INTRODUCTION

Within the Clean Sky framework, a research project, namely TILTOp, is dedicated to the study of air intake and exhaust integration into the ERICA tilt-rotor nacelle [1]-[3] using advanced multi-objective optimization techniques along with CFD.

Efficient aerodynamic design of air intakes is a challenging objective for airframe manufacturers: since the incoming air must be decelerate from flight Mach number to a velocity range suitable for engine compressor operation, the inlet duct must be design to act as a diffuser with gentle diffusion

form flight Mach number to lower Mach number and higher values of static pressure [4]. As a consequence inlet flow is subjected to adverse pressure gradient, which leads to boundary layer instability and possible flow separation. Therefore inlet cross sectional area distribution along the central line should be optimized in order to minimize boundary layer “loading” and avoid separation [5].

In addition, for turboprop intake applications, an S-shaped duct is usually required to channel the air to the engine face; this is due to the presence of the propeller shaft. From the fluid-dynamic point of view, a curved duct induces a secondary flow pattern, which essentially sets up “pockets” of

swirling flow at the duct exit [6] and determines performance degradation of turboprop engines [7], [8]. In severe situations, these pockets of swirling flow can produce rotating stall instability of the compressor rotor [9]. Therefore, the internal shape of the curved duct should embody proper strategies in order to minimize total pressure loss and flow distortion at the engine face [10], [11].

Finally, stability of boundary layer in turboprop inlets may also be remarkably affected by the aircraft operating conditions and flight speed [12], [13], [14].

In such a context CFD is a powerful tool which can be used to accurately evaluate the complex flow behavior within inlet ducts: [15] and [16] are remarkable examples of CFD application to intake aerodynamics. Prior to TILTOp, CFD analyses on the ERICA air intake have been carried out by CENAERO in the framework of the program NICETRIP (a FP7 project funded by EU) [17], [18]. When coupled with geometry parameterization techniques, CFD provides an effective automatic design methodology for inlet ducts. For example, in [19] Zhang et al. describe an automatic design method for 3D subsonic ducts using NURBS.

The TILTOp research program is devoted to the efficient design and the shape optimization of the ERICA tilt-rotor intake and exhaust system, carried out by means of advanced multi-objective optimization algorithms coupled with CFD Navier&Stokes solvers [2]: starting from the existing ERICA nacelle geometry provided by AgustaWestland S.p.A. via CATIA® CAD models, the base-line intake and exhaust CFD model has been built up and validated by means of comparison against the available wind tunnel experimental data. Despite not being modeled directly, the effect of both the engine and the rotor/propeller inflow on the overall installation efficiency has been accounted for. More in detail, the rotor inflow acts as a boundary condition for the intake analysis by means of a non-uniform disk actuator model and also the matching between the intake and the engine has been evaluated; finally, the engine output served as a boundary condition for the exhaust

survey. In this way, the overall propulsion system, including the propeller, the intake, the engine and the exhaust, has been examined in a whole [3]. CFD analysis has been carried out for a series of operating points and obtained results have been analyzed in terms of total pressure losses, flow distortion, flow separation and all those aspects that affect the efficiency of the both the nacelle intake and exhaust [5], in order to identify the most appropriate parametric changes to be applied to the geometry during the optimization phase.

The baseline CFD solution and its associated parametric geometrical shape model are the main inputs for the optimization procedure selected, which involves the application of the innovative code GDEA. The GDEA is the University of Padova homemade genetic algorithm able to perform multi-objective optimization analysis with the general approach of the Pareto frontier search, coupled with HyperMorph® and the CFD solver selected Fluent®.

The GDEA algorithm [28] has been compared to others state of the art genetic algorithm with excellent results and, interfaced with flow solvers, has been successfully used in several fluid-dynamics applications, especially in the field of turbomachinery. See for example [29] and [30] for more elucidations.

The results obtained by the application of this optimization chain on the ERICA nacelle model are presented in this paper, with regards on the air intake optimization outcomes, together with the description of the future work, including engine exhaust optimization, which is going to be addressed to reach the completeness of the TILTOp program on December 2011.

ERICA ENGINE INSTALLATION DESCRIPTION

The ERICA nacelle CAD model pertinent to the engine installation baseline configuration is depicted in Figure 1 and includes:

- External nacelle surfaces;
- Rotor spinner;

- Wing and wing/nacelle junction surfaces;
- Particles separator by-pass;
- Intake duct;
- Exhaust;
- Internal components and transmission gear-box layout;
- Engine layout.

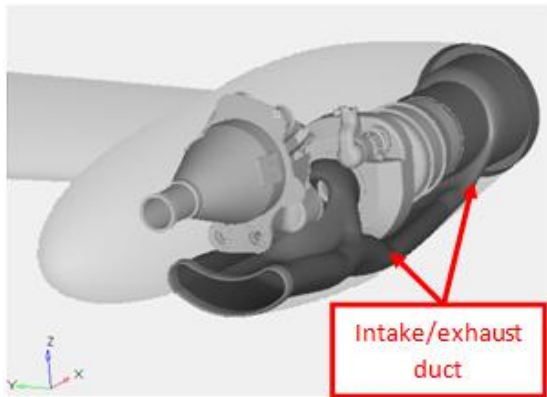


Figure 1: Layout of the ERICA nacelle internal components.

As the reader can notice from Figure 1, the ERICA intake system has a single-scoop inlet, being the intake entry located on the lower part of the aircraft nacelle; the intake lip is characterized by quite a sharp profile, clearly designed to reduce the drag and achieve good intake performance at cruise speed flight conditions; proper design of inlet lip determines performance insensitiveness to pitching, yawing and, above all, swirling flow coming from propellers [20], [21]. The rotor spinner approach surface is physically separated from the inlet by means of a boundary layer diverter, which allows avoiding the ingestion of the approach surface perturbed boundary layer through the inlet. Since the turbo-prop engine must be aligned with the transmission gear-box, as well as because of the single-scoop inlet, a vertical offset exists between the external entry area and the engine face. The single-scoop solution forces the implementation of an S-shaped duct to connect the entry area and the “aerodynamic interface plane” (AIP), which represents the aerodynamic interconnection between the engine face and the intake duct.

The engine power turbine and the transmission gear-box are mechanically connected by means of a power shaft running through the shaft faring. The latter is located within the second bend of the S-shaped duct and its presence makes the engine inlet annular.

Starting from the first bend of the S-shaped duct, a secondary duct goes along the full nacelle span beneath the engine structure, exhausting the ingested air from the nacelle aft wall. This represents the particle by-pass aimed at avoiding foreign object ingestion. The baseline design also includes the engine exhaust duct, i.e. an ejector dedicated to the engine bay ventilation and a main nozzle directly connected to the particle separator by-pass.

ERICA NACELLE CFD MODEL

Starting from the provided CAD models, the surface and volume mesh necessary for the baseline CFD computation have been built up; the main characteristics of the mesh are reported in Table 1.

Surface Mesh	
Mesh type	Triangular
Total Number of elements	~400,000
Element size within the intake & exhaust duct [mm]	2÷15
Element size over the external Nacelle and wing [mm]	5÷35
Volume Mesh	
Mesh type	Hybrid - Unstructured
Boundary layer elements type	Prismatic
Core volume elements type	Tetrahedral
Total number of elements	~6,000,000

Table 1: CFD mesh characteristics.

TAS [m/s]	154
Pressure altitude [m]	7500
OAT [°C]	-33.75
$\mu = V_{\infty}/V_f$	1.4

Table 2: Cruise flight condition.

Only the cruise flight condition has been considered in this paper (μ represents the intake inverse flow ratio [5]); Table 2 reports the main operating conditions taken into account. The external ambient and flight operating conditions have been modeled by means of standard “pressure inlet” and “pressure outlet” boundary conditions implemented within Fluent® [24].

Inlet flow field is strongly dependent on the mass flow rate imposed by the engine compressor at the AIP. The value of AIP mass flow rate is usually a function of both flight operating conditions (flight speed, altitude, external pressure and temperature etc.) and power demanded by the rotor. This situation can be well represented in Fluent® imposing on a surface downstream the AIP a pressure outlet boundary condition with target mass flow rate specification. Such a kind of boundary condition iteratively adjusts the static pressure on the outlet surface until the mass flow rate measured on the same surface matches the specified value [24]. On the exhaust side, a slightly different mass flow rate (differences depend on the fuel flow rate and on compressor bleed flows) must be introduced, at the proper total temperature, from the power turbine exit area. This can be done using a “mass flow inlet” boundary condition [24].

The rotor inflow effect has been taken into account by means of a dedicated non-uniform disc actuator model, applied to the rotor disc surface. Pressure jump and swirl radial profiles, to be applied across the rotor disc, have been provided by AgustaWestland S.p.A specifically for the setup of the Fluent® non-uniform disc actuator model. Figure 2 shows the radial profiles for both pressure jump and swirl (cruise condition).

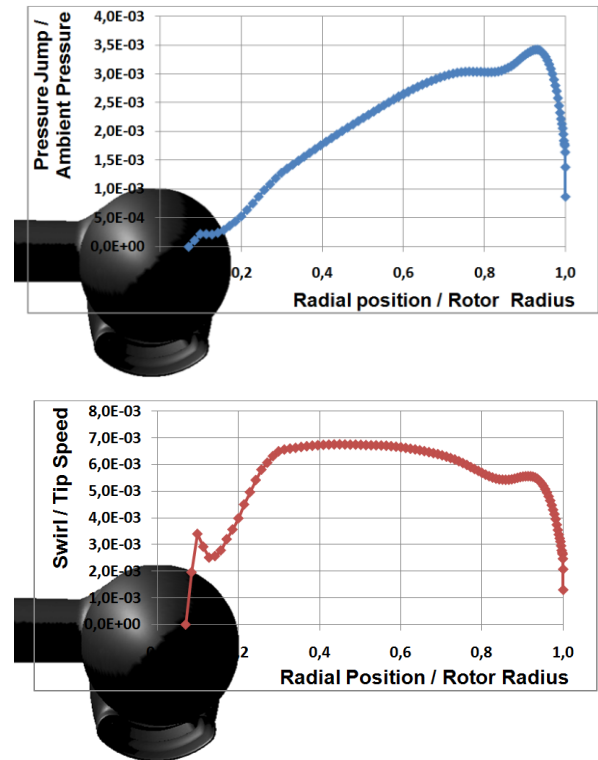


Figure 2: Pressure jump and swirl profiles applied to the rotor disc.

Simulations have been carried out using the following solver settings:

Turbulence model	k- ω SST (two equations)
Density variation law	Ideal gas
Viscosity variation law	Sutherland (three coefficients)
Discretization schemes	All 2 nd order
Near wall treatment	Wall functions

Table 3: Fluent solver settings.

For the present analysis the Wilcox’s two-equation $k-\omega$ model featuring the Menter’s Shear-Stress-Transport correction (SST) (see reference [25], [26]) has been chosen.

Thermodynamic effects have been taken into account by including the energy equation within the

Reynolds Average Navier-Stokes (RANS) system of equations to be solved. The *ideal gas law* is used to properly model density variations as function of pressure and temperature, while the *Sutherland law* is used to compute viscosity variations as function of temperature.

Second order Discretization schemes [24] were used for the final solution; *first order schemes* have been sometimes used during the first part of the computation with the purpose of providing a proper initialization for second order calculation.

The wall function approach has been chosen as near-wall treatment (wall y^+ within the range $30 < y^+ < 300$, [24]) because of its robustness, reliability and reduced computational resources required with respect to the enhanced wall treatment.

The CFD model used for the optimization analysis take advantage of the following design assumption: *geometrical changes on the internal domain do not influence the external domain flow field*. With this in mind it is possible to replace the direct modeling of the external domain with an appropriate set of boundary conditions. Boundary condition data necessary for the application of this approach can be extracted from a dedicated box surfaces specifically included in the complete model used for the baseline performance characterization. Using this method it is possible to obtain a well representative CFD model saving a quite huge number of elements in comparison with the complete model ($\sim 2,000,000$ elements of the design model versus $\sim 6,000,000$ elements of the complete model), while maintaining an adequate solution accuracy.

CFD MODEL VALIDATION

In the period December 2010/January 2011 an experimental campaign, whose purpose was the wind tunnel evaluation of the ERICA intake performance, has been carried out at the POLIMI (Politecnico di Milano) facility in the framework of NICETRIP program. The experimental database provided by this campaign [33] has been used within the TILTOp framework with the purpose of validating the intake CFD model.

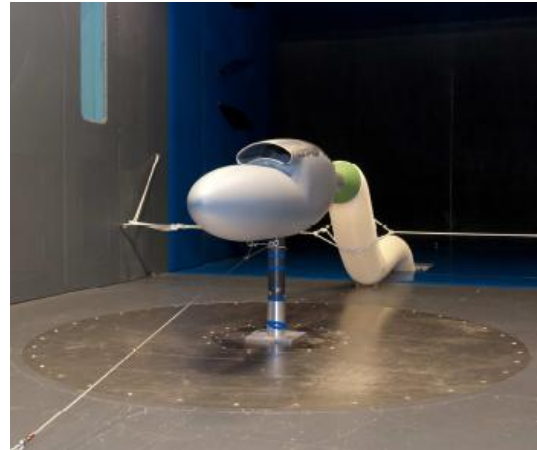


Figure 3: Nacelle model installation in the POLIMI wind tunnel [33].

For this validation task a specific, rotor-less, CFD model has been considered representing the exact wind tunnel geometry and test conditions.

Results have been analyzed in term of total pressure ratio variation as a function of the inverse flow ratio, defined as follows:

$$\mu = \frac{V_{\infty}}{V_f} \quad Eq. 1$$

Where:

- V_{∞} is the free-stream velocity (or wind tunnel velocity in this case);
- V_f is the velocity at AIP. Under the hypothesis of incompressible flow (constant density) the reference value of V_f is determined by the ratio between the volumetric flow rate Q and the AIP area A_f .

The μ parameter depends on both the air speed and the AIP flow rate, which are the two main flow variables; therefore it is often used as the main parameter in intake aerodynamics practice.

In the present work, the total pressure ratio definition is the following [5]:

$$\eta_p = \frac{P_f}{P_{\infty}} \quad Eq. 2$$

Where:

- P_f is total pressure measured at the AIP;
- P_∞ is the free stream total pressure.

Results referring to the cruise tests are reported in the following table.

μ	η_P POLIMI	η_P CFD
0.79	0.996	0.997
1.24	0.995	0.996
1.77	0.997	0.997

Table 4: Experimental and numerical total pressure ratio comparison; cruise flight conditions.

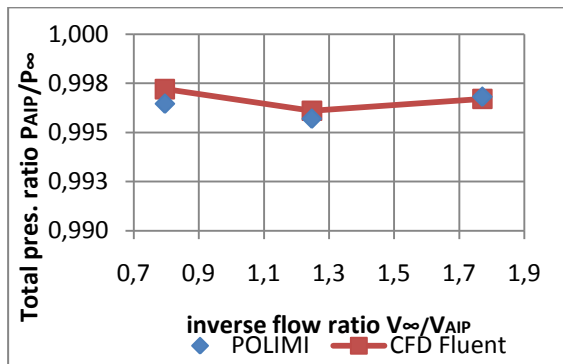


Figure 4: Experimental and numerical total pressure ratio comparison; cruise flight conditions.

Total pressure ratio comparison shows good agreement between experimental data and CFD prediction on the typical cruise inverse flow ratios.

Both static and total pressure distributions have been compared all along the intake duct. Detailed comparison of local static and total pressure data is reported in the TILT_{OP} deliverable D1 [34]; generally experimental trend results to be well captured by CFD simulations, especially on high inverse flow ratio conditions [34].

MAIN FLOW FEATURES AND ASSESSMENT OF THE BASELINE PERFORMANCE PARAMETERS

After CFD model validation, the full scale simulation including the rotor inflow was carried out. This simulation represents the main baseline

configuration assessment; it allows to identify the main flow features characterizing the aerodynamic problem and to determine the baseline performance parameters to be used as reference values for the optimization results.

Within this paper two main performance parameters are considered for intakes:

1. The most common measure of intake efficiency is the intake *total pressure ratio*¹ (Eq. 2). The total pressure ratio represents the efficiency of the intake compression process which transforms the free-stream kinetic energy into static pressure.

A shortfall in efficiency emerges as a loss of total pressure from the free-stream value. If the total pressure loss is denoted by ΔP , we have [5]:

$$\eta_P = 1 - \frac{\Delta P}{P_\infty} \quad \text{Eq. 3}$$

Both total pressure ratio and total pressure loss can be evaluated from CFD simulation by means of standard *Fluent*® post processing functions; in particular P_f can be determined using a mass-weighted-average surface integral (see [24]) of total pressure over the AIP surface, while P_∞ is a boundary value imposed at the virtual wind tunnel inlet. Since those values are known, the computation of both η_P and ΔP is straightforward.

2. The air diffusion process, occurring in the intake system, must be accomplished with the minimum loss in total-pressure and with the best attainable flow distribution at the intake exit plane [22]. Therefore another important intake performance aspect is the AIP flow distortion. For Tilt-Rotor inlets applications, the dominant distortion effect is due to the total pressure distortion.

It is necessary to derive a quantitative measure of distortion, from which both the quality of intake

¹ The total pressure ratio is commonly indicated also with the denomination “pressure recovery”.

flow and the tolerance of an engine can be judged. Distortion coefficients may be defined in various ways; in the UK the usual form is [23]:

$$DC(\theta) = \frac{P_f - P_\theta}{q_f} \quad \text{Eq. 4}$$

Where P_f is the weighted area average total pressure at engine face, q_f is the corresponding mean dynamic head and P_θ is the weighted area average total pressure in the “worst” sector of the face, of angle θ . The sector “ θ ” must be of significant extent and 60° is usually regarded as a satisfactory minimum.



Figure 5: Illustration of total-pressure contours and θ sector for definition of distortion coefficient [5].

Maximum DC60 is adopted by Rolls-Royce as a certification parameter for inlet total pressure distortion and it will be used as the distortion performance parameter throughout the whole document.

CFD computation of DC60 has been carried out by means of a dedicated Fluent Scheme function [32].

In the following the above discussed performance parameter obtained by the CFD assessment of the ERICA intake system baseline configuration are summarized.

Total pressure loss [% of inlet value]	3.71%
DC60 worst sector [θ ; $\theta+60^\circ$]	[60° ; 120°]

Table 5: Baseline intake performance.

Flow distortion behavior can be examined in the following figures where the local DC60 distribution over the AIP surface is shown. The local area weighted average total pressure computed for each sector considered for the DC60

calculation is also reported. θ_x is the azimuth parameter as depicted in Figure 10.

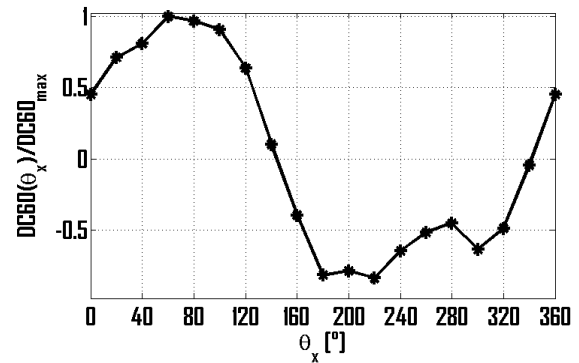


Figure 6: Local DC60 distribution, normalized by the maximum DC60 value.

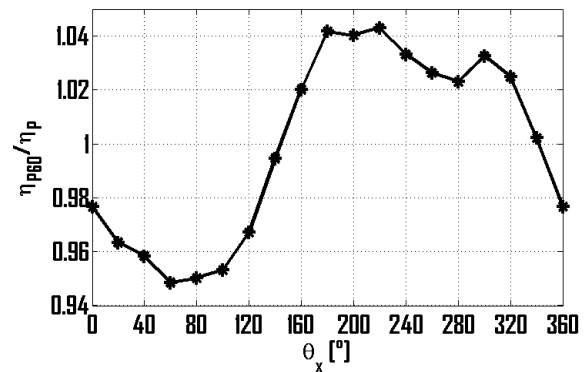


Figure 7: Local values of area weighted average total pressure ratio, normalized by AIP mean total pressure ratio value.

Examination of inlet streamlines demonstrates the good behaviour of the boundary layer diverter: the upper picture in Figure 8 shows in fact that no streamline from the approach surfaces enters through the inlet duct. On the contrary, the high slope S-shaped duct appears to be the major source of losses because of the system of separated flow generated on that region (right picture of Figure 8).

Figure 9 and Figure 10 point out the two main loss and distortion mechanisms. In particular flow separation induced by the S-duct slope represents the main source of total pressure loss and distortion, while the obliquely reattaching flow on the inner radius of the S-duct second bend causes also a non-symmetric distribution of total pressure at the AIP, which is an additional source of distortion.

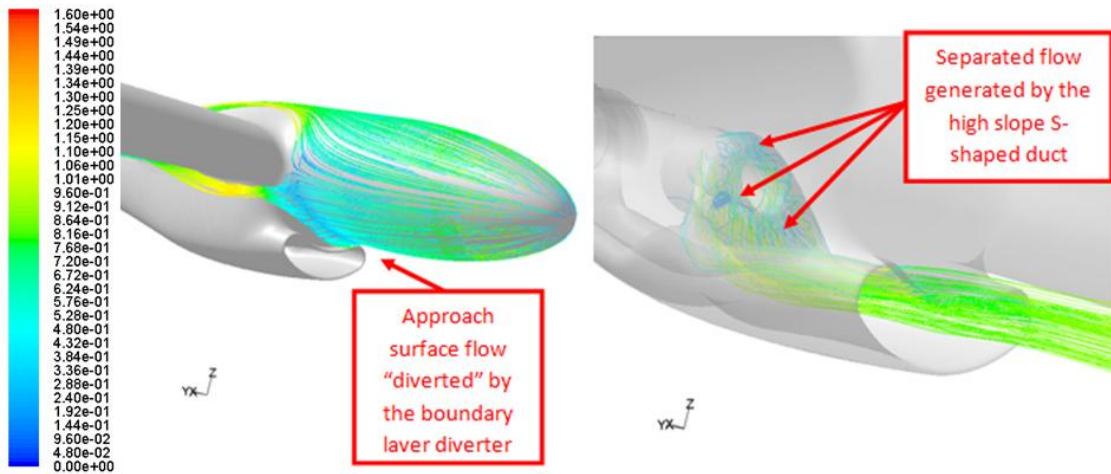


Figure 8: Streamlines (colored by velocity magnitude, normalized by free stream velocity) over the external nacelle and the intake duct.

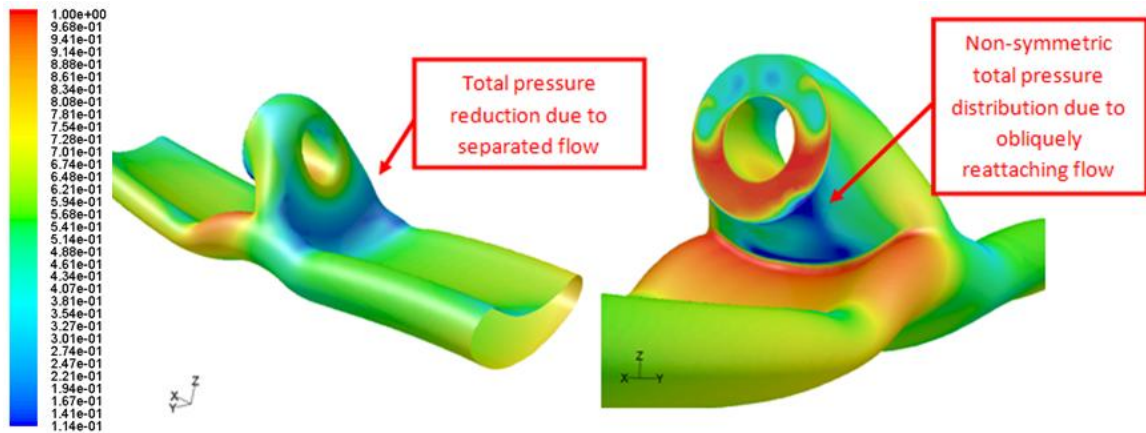


Figure 9: Total pressure contours over the intake duct (normalized by free stream total pressure value).

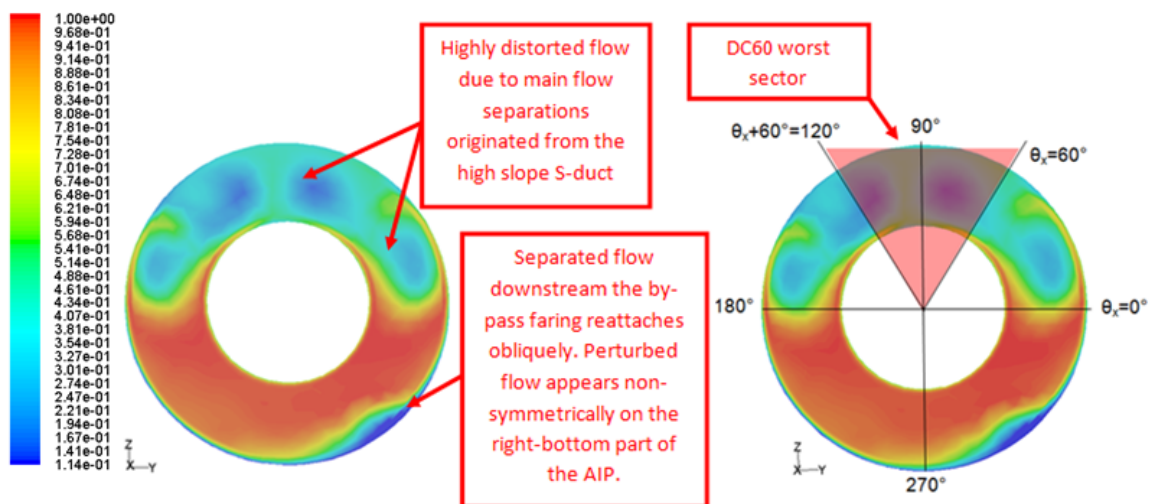


Figure 10: AIP total pressure distribution (normalized by free stream total pressure value).

DESCRIPTION OF THE OPTIMIZATION METHOD

The aerodynamic optimization procedure which has been implemented and is used for the project TILTOp is structured in three phases as follows:

- 1) Baseline model preparation and simulation phase;
- 2) Automatic optimization phase;
- 3) Post-processing and optimized CAD model reconstruction phase.

A detailed description of the GDEA based optimization loop is reported in the associated TILTOp deliverables [35], [36].

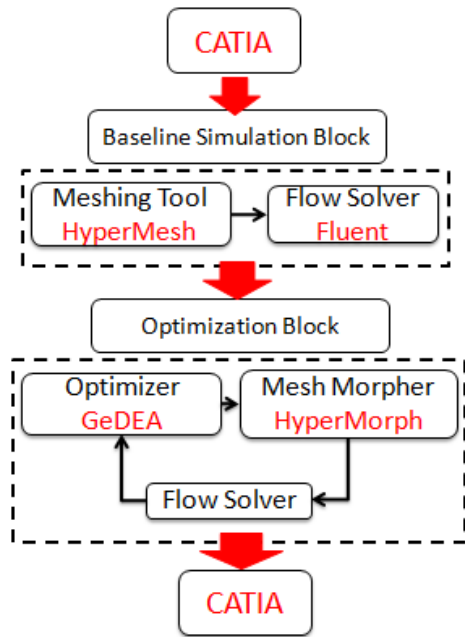


Figure 11: Optimization method flow-chart.

Baseline model simulation

Typically the starting point is represented by the CAD model of the baseline configuration. Starting from the geometrical model, the procedure moves into the “baseline simulation block” (see Figure 11), where the baseline configuration of the component under consideration must be analyzed, in terms of aerodynamic performance in the most

relevant operating conditions, via CFD computation using the selected flow solver. The assessment of the baseline solution allows the designer to properly understand the flow field characteristics of the object under analysis, gives fundamental indications for the optimization objectives and constraints identification and allows to properly setting up the geometrical parametric model.

Automatic optimization execution

When the preliminary operations have been completed, the optimization can be carried out by means of the automatic optimization loop in Figure 11: it is constituted by the following components:

- 1) GDEA (Genetic Diversity Evolutionary Algorithm): it is an advanced multi-objective optimization algorithm developed at the University of Padova [28]. It is the selected optimization engine;
- 2) Altair HyperMorph®: it makes it possible to convert the design parameters coming out from GDEA into morphed CFD cases, suitable for the objective function evaluation;
- 3) Ansys Fluent®: the selected flow solver; it takes in input the morphed CFD cases coming from HyperMorph® and gives back to GDEA the correspondent values of the chosen objective functions.

During the optimization process, GDEA let a population of individuals “evolve” (each one corresponding to a different set of design variables and so to a different geometry configuration) until the convergence to the *Pareto optimal frontier* has been reached, being the Pareto frontier the set of non-inferior solutions, which represents the solution of a multi-objective optimization problem; a non-inferior solution, also called Pareto optimal or non-dominated solution, is one in which an improvement in one objective requires the degradation of another [31].

Post-processing

The Pareto frontier in output from the automatic optimization loop represents a multiple set of solutions equally optimal according to the Pareto

concept but of course different from the aerodynamic and engineering point of view. In fact each solution over the Pareto frontier may present advantages and drawbacks with respect to the other solutions. In order to choose among the optimal set the most appropriate solution a post-processing work is necessary. Thanks to the intrinsic multi-objective approach adopted, the designer is allowed to select, among the Pareto optimal set, the solution which is more suitable for his needs: for example, choosing to privilege the improvement of one objective with respect to the other or even including other considerations such as non-aerodynamic requirements. The strength of the selected approach is that the designer can choose the proper trade-off between the objectives when the optimization work has been completed and he is not forced to introduce his arbitrariness in the problem set up, as commonly happens using traditional optimization approaches.

SET-UP OF THE PARAMETRIC MODEL

Looking at the baseline simulation results described within the previous sections it is clear that the main source of total pressure losses and flow distortion is the high slope bend which characterizes the S-shaped duct of the ERICA intake. In order to optimize the intake design it is therefore necessary to modify the geometry of that region: modifications of both the duct center line and cross-sectional shape have been included because of their effect on inlet performance [5], [15]. Eight design parameters have been identified for the geometrical control of the S-duct surfaces; they are shortly described in Table 6.

Those parametric shapes have been generated using the Altair software HyperMesh® by means of the mesh morphing and parameterization techniques available within the morphing toolbox HyperMorph®. The morphing method selected for the current application is the *domain/handles* approach [27], which allows the application of mesh nodes displacements within a geometrical region (domain) by changing the location of specific, user defined, control points (handles).

Design Parameter	Description
Sh1	Second bend inner surface shape
Sh2	By-pass duct shape
Sh3	Entry duct shape
Sh4	S-connection “x” position
Sh5	First bend inner surface shape
Sh6	First bend outer surface shape
Sh7	Second bend outer surface shape (upper part)
Sh8	Second bend outer surface shape, (lower part)

Table 6: Intake duct design parameters summary.

When applied, the nodes displacements can be saved as perturbation vectors and then be reapplied to the baseline model with any given scaling factor. The reader can visualize the $x - z$ plane cuts of the intake model parametric shapes, applied with the basic scaling factor equal to one, from Figure 12 to Figure 19; the corresponding handle displacements are visualized also. In the Figures the black and red lines represent respectively the baseline and morphed $x-z$ cut view of the intake duct. The handles initial and final positions are marked respectively with the yellow and green dots. The blue arrow represents the handle displacement, which is also indicated by components (normalized by the AIP radius) at the top left of the Figures.

The morphed geometry results from the linear combination of the user defined shapes multiplied by their own scaling factors:

$$\mathbf{v} = \sum_{i=1}^8 \alpha_i Sh_i \quad Eq. 5$$

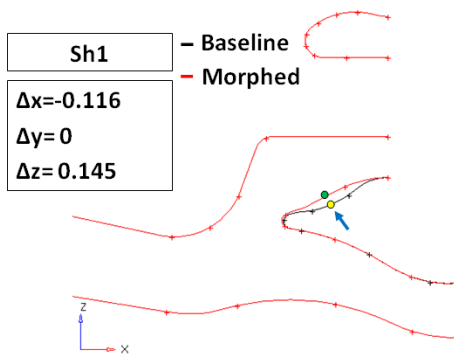


Figure 12: Parametric shape Sh1, applied to the intake model with scaling factor $\alpha_1=1$

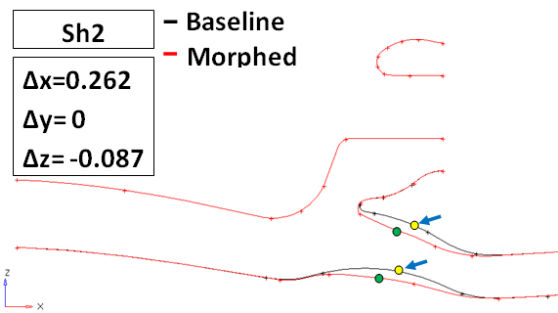


Figure 13: Parametric shape Sh2, applied to the intake model with scaling factor $\alpha_2=1$.

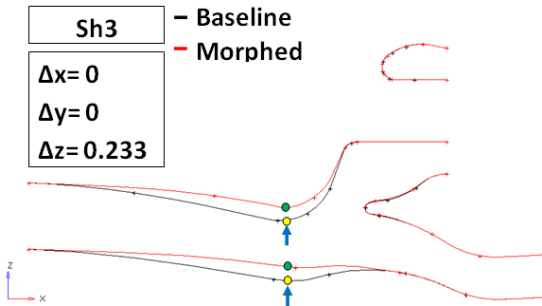


Figure 14: Parametric shape Sh3, applied to the intake model with scaling factor $\alpha_3=1$.

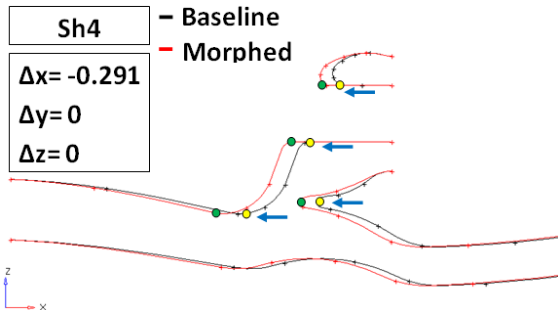


Figure 15: Parametric shape Sh4, applied to the intake model with scaling factor $\alpha_4=1$.

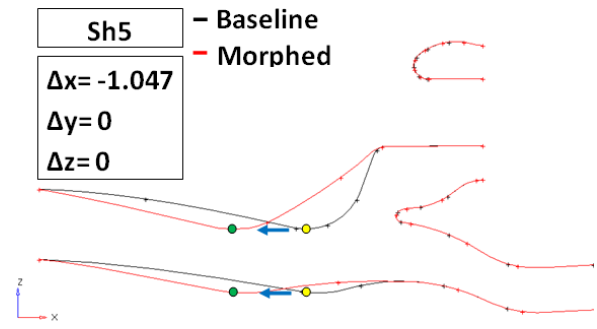


Figure 16: Parametric shape Sh5, applied to the intake model with scaling factor $\alpha_5=1$.

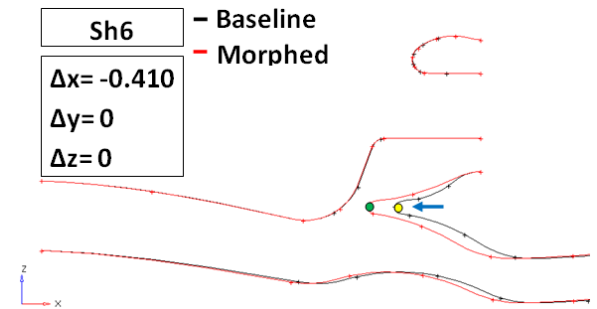


Figure 17: Parametric shape Sh6, applied to the intake model with scaling factor $\alpha_6=1$.

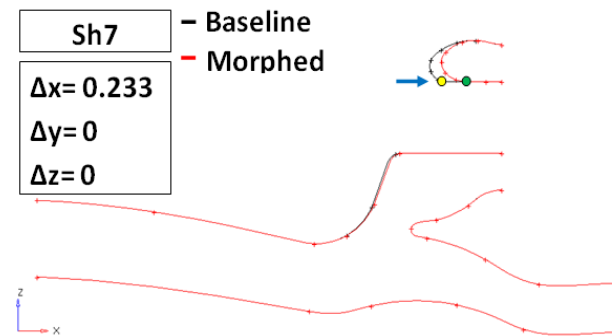


Figure 18: Parametric shape Sh7, applied to the intake model with scaling factor $\alpha_7=1$.

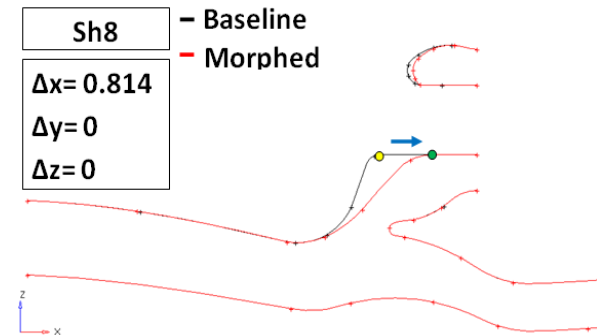


Figure 19: Parametric shape Sh8, applied to the intake model with scaling factor $\alpha_8=1$.

Where:

- \mathbf{v} the global displacement vector;
- Sh_i is the i^{th} basic shape as visualized in Figure 12 to Figure 19;
- α_i is the i^{th} shape scaling factor and it is generated by GDEA.

For the present application the α_i factors are defined within the following range:

$$\begin{aligned} \alpha_i &\in [0; 1], i = 1,3,4,5,7,8 \\ \alpha_i &\in [-1; 1], i = 2,6 \end{aligned} \quad \text{Eq. 6}$$

Using this approach, a scaling factor equal to zero means the morphed geometry results to be identical to the baseline one, while a scaling factor equal to one produce the maximum displacement as shown in the previous Figures. Scaling factors equal to minus one produce the maximum displacement but in the opposite direction with respect to what is represented on the Figures.

The maximum displacements have been chosen such as to avoid collisions between the morphed surfaces and the other nacelle internal components i.e. the engine, the transmission gearbox and the other accessories, as well as the nacelle external surfaces.

Two additional morphing constraints have been added to the parametric model:

1. Nodes located the AIP surface are constrained to stay fixed on their location in order to not change the engine position;
2. Nodes located on the internal surface of the power shaft fairing are constrained to translate only along the “x” direction in order to avoid interferences between the morphed surfaces and the power shaft.

FORMULATION OF THE OPTIMIZATION PROBLEM

When both the design CFD model and the parametric model for the intake geometry are ready,

the last step is the GDEA optimization problem formulation. It can be expressed in the following way:

$$\text{Maximize}[\mathbf{F}(\mathbf{x})] \quad \text{Eq. 7}$$

Where:

- $\mathbf{F}(\mathbf{x}) = [\eta_p, -DC60]$;
- $\mathbf{x} = [\alpha_1, \alpha_2, \alpha_3, \alpha_4, \alpha_5, \alpha_6, \alpha_7, \alpha_8]$.

Subject to the variables bounds:

$$\begin{aligned} \alpha_i &\in [0; 1], i = 1,3,4,5,7,8 \\ \alpha_i &\in [-1; 1], i = 2,6 \end{aligned}$$

As explained in the previous section, the design parameters vector affects the baseline geometry by means of the HyperMorph shapes (Sh_i , $i=1\dots 8$) application, resulting in the morphed configuration:

$$\mathbf{v}(\mathbf{x}) = \sum_{i=1}^8 \alpha_i Sh_i \quad \text{Eq. 8}$$

Thanks to this bi-objective formulation, the optimization algorithm seeks for solutions presenting improved performance in terms of both total pressure ratio and total pressure flow distortion.

The number of individuals per generation has been set to 40, while a total number of ten generations has been considered for the preliminary optimization run.

INTAKE OPTIMIZATION RESULTS

The intake optimization results are discussed within this section; even if the optimization procedure has been run only for a small number of generations, remarkable improvements can be observed on both the objective functions considered.

The Figure below shows the Pareto frontier calculated by the GDEA algorithm after ten generations:

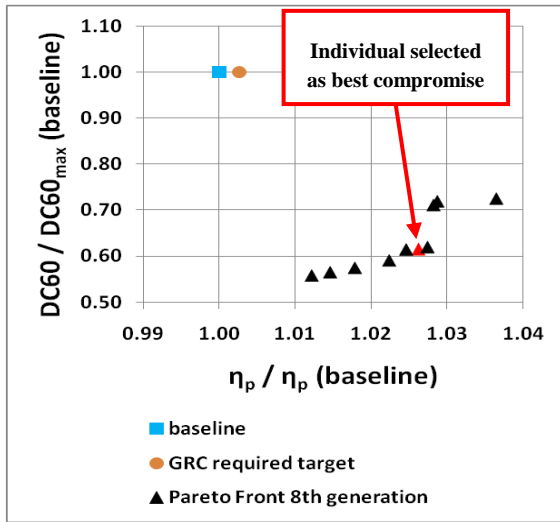


Figure 20: GDEA Pareto frontier, 10th generation; the selected optimal individual is highlighted in red.

In particular the possible reduction in total pressure loss is much bigger than the target required by the Green Rotorcraft Consortium (GRC), which was estimated as the 5% of the baseline loss value [37] and it corresponds to the orange point in Figure 20. Moreover the resulting optimized solutions are characterized by a much lower distortion level with respect to baseline as the reduction of the DC60 parameter shows.

solution	Baseline	GRC target	Optimized
DC60/DC60max (baseline)	1	1	0.619
Total pressure loss (% of inlet value)	3.71%	3.52%	1.40%
DC60 reduction respect to baseline [%]	/	/	38.04%
Loss reduction respect to baseline [%]	/	5.00%	52.00%

Table 7: Objectives comparison between the baseline and optimized configuration.

Since it is a good compromise between the two objectives, the red point in Figure 20 has been chosen for further discussion and comparison within the paper; Table 7 shows a detailed objective comparison between this optimal solution, the baseline and the GRC required target.

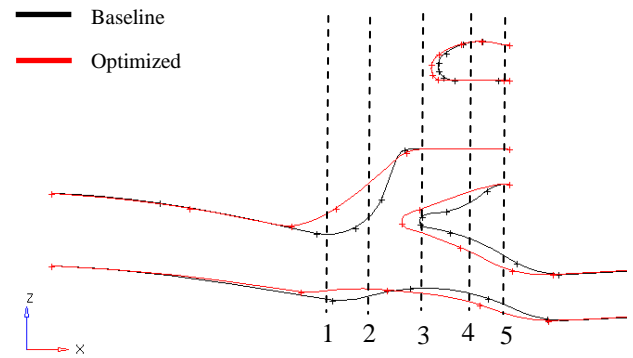


Figure 21: Comparison between baseline (black) and optimal (red) duct geometry; x-z plane section.

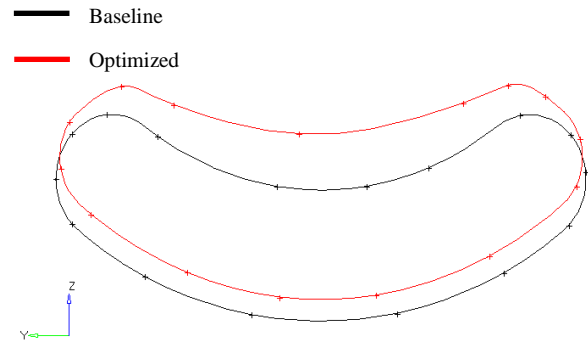


Figure 22: Comparison between baseline and optimal duct geometry; transversal section 1.

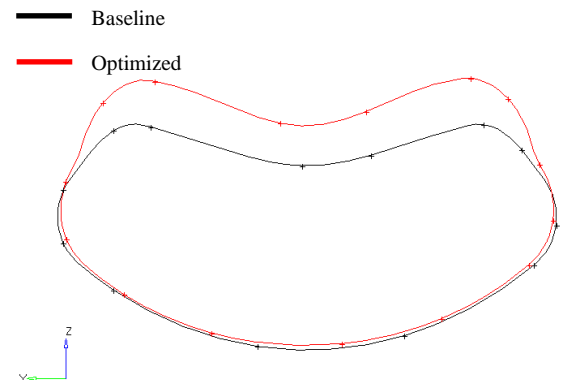


Figure 23: Comparison between baseline and optimal duct geometry; transversal section 2.

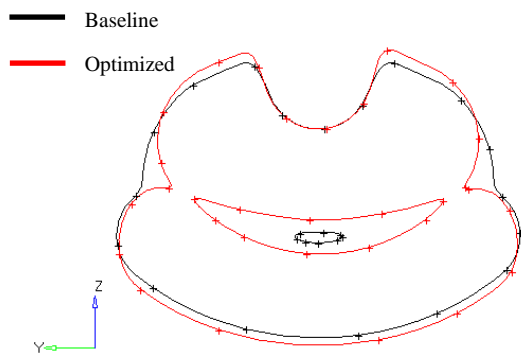


Figure 24: Comparison between baseline and optimal duct geometry; transversal section 3.

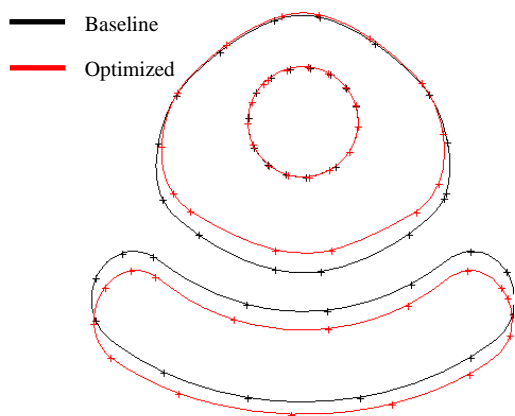


Figure 25: Comparison between baseline and optimal duct geometry; transversal section 4.

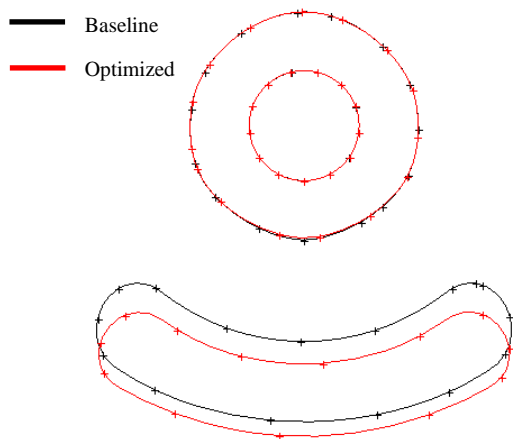


Figure 26: Comparison between baseline and optimal duct geometry; transversal section 5.

Looking at the geometry comparison it is possible to notice that the optimal configuration presents a smoother curvature of the duct central line, tending to reduce the slope of the S-duct;

moreover the transversal section area variation along the duct central line is more gradual with respect to baseline, resulting in a lower intensity of the adverse pressure gradient along the duct: this effect reduces both the extent and the intensity of the separated flow region at the duct S-bend (Figure 27) leading to a more uniform total pressure distribution at AIP (Figure 28). Comparisons of local DC60 and local AIP sector average total pressure distribution show the much more uniform total pressure pattern at the engine face. This result, together with the higher AIP total pressure average value, is expected to greatly improve the engine performance and stability.

FUTURE TILT TOP WORK

After the completion of the intake optimization, the performance of the optimal configurations in different flight conditions will be compared against the baseline geometry simulation results: according to the Clean Sky Green Rotorcraft requirements, the flight conditions considered will be the hover and three conversion modes. Special care will be dedicated to the low velocity conversion flight where strong lip separation effects have been observed during the characterization phase [34]. A parametric model of the lip region will be built up and the influence of geometrical parameters such as lip shape and stagger angle on intake performance at incidence will be investigated. If necessary a GDEA optimization will be executed in order to improve the intake behaviour at low velocity conversion condition.

A GDEA optimization will be executed even on the ERICA engine exhaust system. The most critical condition for the exhaust is the hover case, where exhaust back pressure should be minimized in order to reduce the engine power output penalty resulting from back pressure. An important constraint for this optimization problem is represented by the particle separator efficiency, which, especially in hover conditions, is strongly dependent by the ejector duct geometrical parameters such as the ejector length and exhaust final diameter.

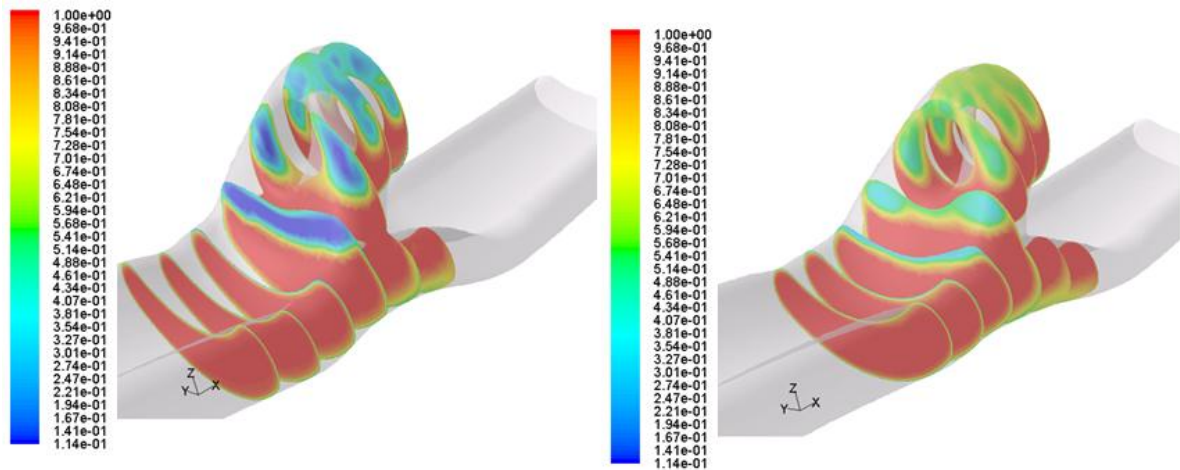


Figure 27: Total pressure distribution along the duct (normalized by free stream total pressure value); baseline (left) and optimal configuration (right).

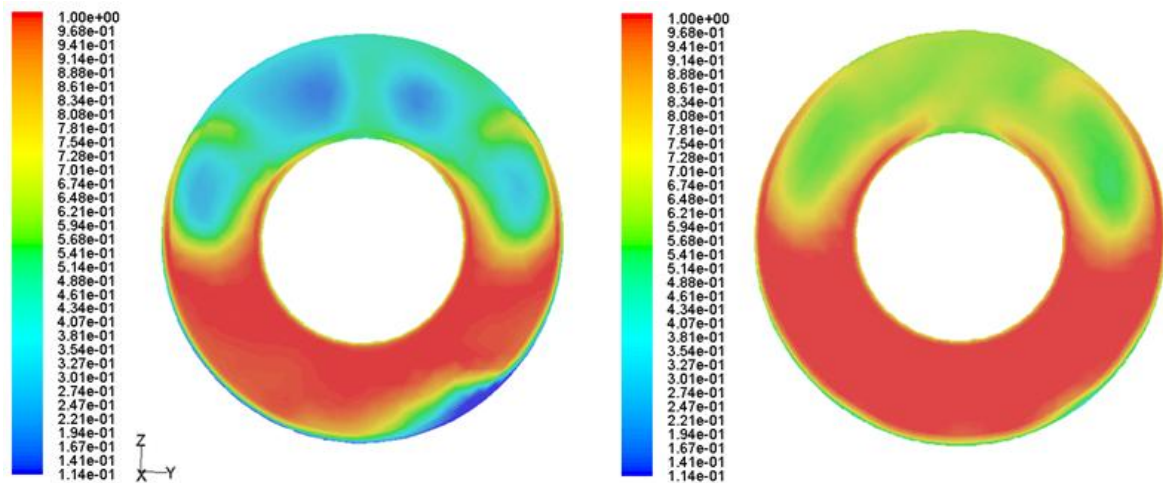


Figure 28: AIP total pressure distribution comparison (normalized by free stream total pressure value); baseline (left) and optimal solution (right).

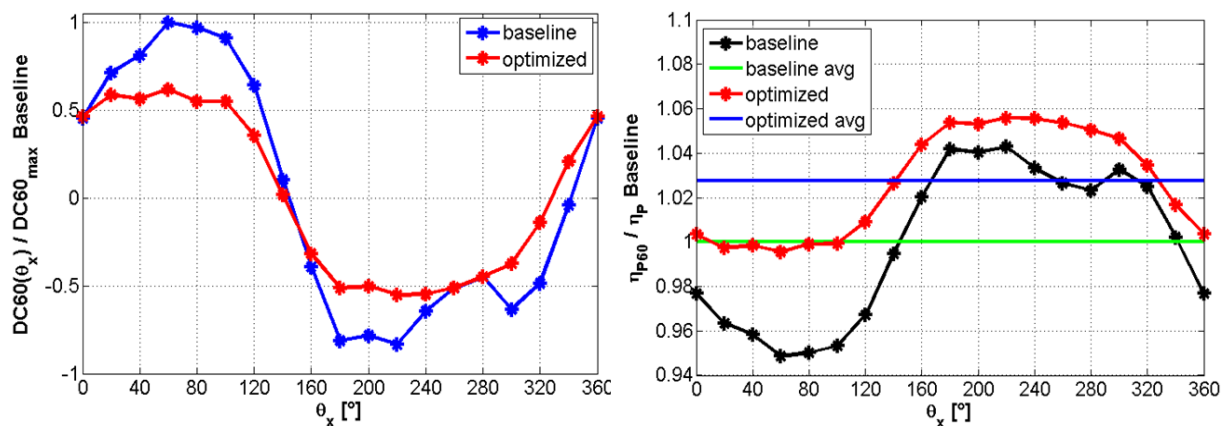


Figure 29: Local DC60 comparison (left) and local sector average total pressure comparison (right) between baseline and optimal configuration. Global AIP average values are also shown on the right.

CONCLUDING REMARKS

The present paper summarizes the main outcomes of the TILTOp program, regarding the efficient design and optimization of the ERICA tilt-rotor engine air intake. The GDEA based optimization loop has been applied to the intake duct parametric model and ten genetic algorithm generations have been completed at the time this paper has been submitted. Results presented within the paper already show an important improvement of the air intake aerodynamic behaviour in term of both total pressure loss and total pressure distortion. In particular the reduction of total pressure loss is already compliant with the Green Rotorcraft Consortium requirements (5% reduction with respect to the baseline configuration [37]) for the most of the solutions among the Pareto frontier.

The discussion reported within the paper demonstrates the strength of the parametric approach chosen: the genetic algorithm GDEA provides an efficient and fully automatic search procedure for optimal solutions, while the coupling with CFD flow solvers allows the accurate evaluation of aerodynamic objective functions. Moreover, the morphing technology adopted allows solutions compatibility with feasibility considerations and industrial constraints. The remarkable improvements of the ERICA intake performances prove the method effectiveness.

ACKNOWLEDGMENTS

This research activity is partially funded by the Clean Sky Joint Undertaking under projects GAM-GRC, related to activities performed within the ITD Green Rotorcraft. The authors would like to thank Dr. Sebastian Dubois of the Clean Sky Joint Undertaking for the management monitoring of the TILTOp program.

REFERENCES

- [1] **Fabio Nannoni, Giorgio Giancamilli, and Marco Cicalè.** *Erica: the European advance tilt-rotor.* 27th European Rotorcraft Forum, Moscow, Russia, 11th – 14th September 2001.
- [2] Clean Sky Joint Undertaking Call for Proposals: SP1-JTI-CS-2009-02. Issue date 25-12-2009.
- [3] **Benini, Ernesto and Ponza, Rita.** *TILTOp Proposal.* JTI-CS-2009-2-GRC-02-001.
- [4] **Hill, P., Peterson, C.,** *Mechanics and Thermodynamics of Propulsion,* Addison-Wesley Publishing Company, 1992.
- [5] **Seddon J. and Goldsmith L.** *Intake Aerodynamics.* Blackwell Science, 2 edition, 1999.
- [6] **Seddon, J.,** “*Understanding and countering the swirl in S-ducts: tests on the sensitivity of swirl to fences,*” *Aeronautical Journal,* R.Ae.Soc., 1984.
- [7] **Detra, R.W.,** “*The secondary Flow in Curved Pipes,*” PhD Thesis, ETH Zurich, 1953.
- [8] **Aulehla, F., Schmitz, D.M.,** “*Intake swirl and simplified methods for dynamic pressure distortion assessment,*” in *Intake Aerodynamics,* VKI Lecture Series, 1988.
- [9] **Farokhi, S.,** *Aircraft propulsion,* John Wiley & Sons, Inc. 2009.
- [10] **Guo, R. W. and Seddon, J.,** “*Some unsteady flow characteristics of two S-shaped intake models tested at high incidence,*” University of Bristol, Department of Aeronautical Engineering, Report No. RWG/JS/3/82, 1982.
- [11] **FriP. Chudý, P., Filakovský, K., Friedl** (2004). *Aerodynamic Analysis of Turboprop Engine Air Intake,* Acta Polytechnica Vol. 44 No. 3.
- [12] **Anderson, B.H.,** “*Inlets, Ducts and Nozzles,*” Proceedings of Aeropropulsion '87, NASA CP-3049, 1987.
- [13] **Sinha, R.,** “*Transient Inlet Nacelle Code,*” *AIAA Journal of Propulsion and Power,* 4, pp. 252-255, 1988.
- [14] **Küchemann, D., Weber, J.,** *Aerodynamics of Propulsion,* New York: McGrawHill, 1953.
- [15] **Saha, K., Singh, S.N. and Seshadri, V.** (2007). *Computational Analysis on Flow Through Transition S-Diffusers: Effect of*

- Inlet Shape*, AIAA, Journal of Aircraft, Vol. 44, No.
- [16] **Robichaud, M. P., Di Bartolomeo, Heikurinen, W., Habashi, W.G.** (1997). *Turboprop air intake design using 3-D viscous analysis*, AIAA, Aerospace Sciences Meeting & Exhibit, 35th, Reno, NV.
- [17] **T. Louagie**, Cenaero, *Preliminary CFD results on the nacelle/intake*. NICETRIP T4.5.1.
- [18] **Philippe Geuzaine**. NICETRIP WP4.5: Progress meeting on sep 14, 2009 at Eurocopter (Marseille).CFD-MP Group, Cenaero.
- [19] **Zhang, W. L., Knight, D. D., Smith, D.** (2000). *Automated Design of a Three-Dimensional Subsonic Diffuser*, Journal Of Propulsion And Power, Vol. 16, No. 6.
- [20] **Hancock, J.P. Lyman, V., Pennock, A.P.**, "Analysis of Results from Wind Tunnel Tests of Inlets for an Advanced Turboprop Nacelle Installation, Q NASA Contractor Report 174937, 1986.
- [21] Final Report for NASA Contract NAS3-22751: "Aerodynamic and Mechanical Design of Advanced Turboprop Core Inlets for the NASA-Lewis PTR," Lockheed-Georgia Company LG83ER0136, 1983.
- [22] **Oates, G.C.**, "Aircraft Propulsion Systems Technology and Design," AIAA Education Series 1989.
- [23] **K. Hünecke**, "Jet engines: fundamentals of theory, design, and operation," Motorbooks International Publishers & Wholesalers, 1997.
- [24] Ansys Fluent 12.0.16 User Guide.
- [25] **D.C. Wilcox**. *Turbulence Modeling for CFD*. DCW Industries, Inc., La Canada, California, 1998.
- [26] **Menter, F. R.**, "Two-Equation Eddy-Viscosity Turbulence Models for Engineering Applications," AIAA Journal, Vol. 32, No. 8, August 1994, pp. 1598-1605.
- [27] Altair HyperMesh 9.0 User Guide.
- [28] **Benini, E. and Toffolo, A.** *Genetic diversity as an objective in multi-objective evolutionary algorithms*. Evolutionary Computation, MIT press journal, 11(2):151–167, 2003.
- [29] **Benini, E. and Toffolo A.** (2002a). *Development of high-performance airfoils for axial flow compressors using evolutionary computation*. AIAA Journal for Propulsion and Power, 18(3):544-554.
- [30] **Benini, E.**, *Multi-objective Design Optimization of a Transonic Compressor Rotor using Evolutionary Computation*, AIAA paper 2003-4090.
- [31] **Deb K.** *Multi-Objective Optimization Using Evolutionary Algorithms*. Wiley, 2001.
- [32] **Mirko Javurek**. *Scheme Programming in FLUENT 5 & 6*. Institut für Strömungsprozesse und Wärmeübertragung, Johannes Kepler Universität Linz, Österreich, September 2000.
- [33] **G. Campanardi, G. Gibertini**. *Nacelle air intake preliminary wind tunnel tests*. NICETRIP/POLIMI/WP4.TR015/1.0.
- [34] **Andrea Garavello**. *TILT_{Op} Deliverable D1: Familiarization with the current engine/nacelle integration and definition of the baseline properties*. Document n. CS/TT/HIT09/WP1.1/1/A.
- [35] **Andrea Garavello**. *CODETilt Deliverable D1 part II: Release of the optimization Software package*. Document n. CS/CT/HIT09/WP1.2/1/A.
- [36] **Andrea Garavello**. *Optimization Software User Manual*. Document n. CS/TT/HIT09/WP1.2/1/A.
- [37] **C.Cassinelli, A.Saporiti (Agusta)**, Content Approval J. Decours (ONERA), P. Vitagliano (CIRA). *GRC-ITD Grant Agreement n°: CSJU-GAM-GRC-2008-001, Specification of optimization targets, operating points and geometrical constraints*. Issue date 25-06-2010.